Applied Energy 285 (2021) 116414

Contents lists available at ScienceDirect

Applied Energy

journal homepage: www.elsevier.com/locate/apenergy

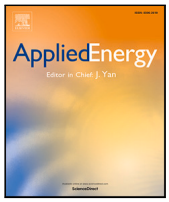

Emission limited model predictive control of a small-scale biomass furnace

Lukas Böhler [a,*], Markus Fallmann [a], Gregor Görtler [b], Jürgen Krail [b], Florian Schittl [b], Martin Kozek [a]

[a] TU Wien, Institute of Mechanics and Mechatronics, 1060 Vienna, Austria
[b] Fachhochschule Burgenland GmbH, 7423 Pinkafeld, Austria

ARTICLE INFO

Keywords:
Biomass combustion
Combustion modeling
Emission reduction
Predictive control
Carbon monoxide

ABSTRACT

This paper presents the application of an emission limiting model-based predictive controller for a small-scale biomass grate furnace. The furnace has a nominal power of 100 kW with wood pellets as fuel, but it can be operated with different fuels as well. The model predictive approach extends the existing static feedforward controller of the investigated furnace with a dynamic feedback controller that is able to improve the combustion performance. Simultaneously, the formation of carbon monoxide emissions is minimized within the prediction horizon based on an available emission estimation model for pellets. The results obtained from closed-loop measurements show that the control concept is able to reduce carbon monoxide emissions in partial load operation up to four times while the control error of the supply water temperature for heating is nearly halved during transient operation. This is achieved by incorporating the emission estimation model into the constrained optimization of the predictive controller. Additional results obtained from closed-loop experiments for different fuel types with varying water contents demonstrate the advantages of the proposed model-based approach and its robustness with respect to typical uncertainties of the combustion process.

1. Introduction

While modern furnace designs are optimized with the latest development tools, their integrated control algorithms are still often realized with classical PID-based methods. A major reason is their simplicity and robustness while requiring only a basic understanding of control engineering and little maintenance effort. As the requirements for combustion increase, especially with respect to efficiency and emission limitations, the requirements for furnace control increase as well. Varying fuel properties, complex underlying process models and highly specific furnace designs however inhibit the implementation of advanced control algorithms. This work therefore proposes the application of a model predictive controller (MPC) for the considered furnace.

The goal is to design a simple and effective model-based controller, which specifically reduces carbon monoxide (CO) emissions in all operating points and increases the fuel flexibility without the loss of performance. Limiting emissions based on primary measures is economically more alluring for small-scale furnaces compared to retrofitting each individual plant with filters. This work introduces the combination of a process model and a carbon monoxide estimation model for control, resulting in a novel CO emission limiting predictive controller without requiring additional measurements. Performance measures quantitatively validate the emission model and the efficiency of the controller. Moreover, they highlight that the targeted CO limiting strategy and fuel flexibility are in fact achieved.

Emission limiting combustion control has already been introduced over two decades ago in [1] for the control of a municipal waste incinerator. Surveys have been performed regarding the emission formation of CO and nitrogen oxides (NO_x) at the incinerator. These observations have been translated into a linguistic fuzzy-rule based controller. A similar approach is later presented in [2], which introduces a hierarchical fuzzy-rule based control concept to prevent the formation of CO in a 200 kW stoker burner for wood chips. Even if successfully realized, both approaches lack process or emission formation models which prevents further application of more advanced control concepts. In [3] an RBF-ARX model-based MPC is introduced for a 375 MW oil fired electric power plant which incorporates the NO_x decomposition of the process. Although the presented predictive approach is generic, it requires an extensive identification and model selection process that results in several local linear black-box models of a specific system. For the investigated furnace a distinct process model [4] and a CO estimation model [5] are available, which provide the basis for a more transparent control design. Although literature suggests the application of fuzzy or nonlinear methods, one MPC is sufficient to cover the entire

* Corresponding author.
E-mail address: lukas.boehler@tuwien.ac.at (L. Böhler).

https://doi.org/10.1016/j.apenergy.2020.116414
Received 5 August 2020; Received in revised form 20 December 2020; Accepted 27 December 2020
Available online 12 January 2021

operating range if adequately set up. This is facilitated by a feedforward controller that compensates most of the static nonlinearities of the investigated plant. Thus, a linear predictive controller based on the available model and linearized around one operating point determined by the ν-gap metric [6] is considered.

Model-based control concepts evolving around input-out-put linearization and decoupling addressing similar issues have been derived in [7] for medium-scale and adapted in [8] for small-scale furnaces. Consecutive works are presented for example in [9], presenting internal model control, or in [10], showing that these concepts can be applied to large-scale furnaces as well. As addressed in [11], constraints for input–output linearization based approaches have to be taken into account by trajectory planning. Handling constraints or anti-windup effects is however already incorporated in standard MPC formulations. Successfully applied predictive controllers are presented in [12] for the combustion of waste or in [13] for a 5MW furnace for the combustion of wood chips. Depending on the model and control complexity though, the optimization conducted by the MPC can lead to computational loads potentially exceeding the capabilities of small furnaces, which is hardly an issue for dynamic feedforward control. The emission limiting MPC concept proposed in this work therefore aims to prevent high calculation efforts by using a simple linearized process model and only the most essential extensions to consider emission formation and saturations.

Emission reduced control requires a basic understanding of emission formation and how it can be made accessible for control. The formation of emissions depends on several factors, like the elemental composition of the fuel, the combustion technology [14] or the operating conditions [15]. The combustion can be described in detail by stoichiometric relations, as presented in [16], or be derived from observations and measurements as in [14] or [17] for different combustion technologies and fuels. While stoichiometric approaches require knowledge about the combustion reactants [18], which is often not available, observations can be gathered to derive data-driven models. Static approaches are presented in [15] for instance which can be especially useful to identify optimal steady-state operating conditions for minimal emissions. Comprehensive data on the influence of excess air and temperature on the formation of emissions, including CO and NO_x, is collected and presented in [19] for a small-scale grate furnace. These surveys only allow for furnace-specific statements regarding emission reduction since the variation of technology and fuel has a major influence on emission formation. Dynamic models allow transient process descriptions but are more difficult to obtain. This is typically addressed by the application of black-box models, for which an overview is given in [20]. Estimation models specifically for CO are derived and compared in [5] for the combustion of wood pellets or in [21] for lump coal. Both, dynamic and static emission estimation models, can be integrated into the MPC by different means in order to achieve emission limited combustion.

In order to design the furnace controller, a simple but descriptive process model is required. Approaches with distributed parameters, as presented in [22] for fixed-bed combustion of biofuels, for example, are typically too complex for control. Various process models are available in literature apart from those already addressed in the context of control. For example, [23] presented a model specifically designed for optimal control applications and [24] provided a compact set of equations for small furnaces as well. The considered combustion model is obtained from [4] and adjusted based on measurements since it is already tailored to the investigated furnace.

This paper is structured as follows: First, the furnace design and the governing equations for the process model are introduced and described together with a short recap about emission formation in small furnaces. Next, the application of the MPC is illustrated and discussed in detail, followed by the introduction of the control algorithm. Then, closed-loop results are shown based on wood pellets and consecutively for different fuels. Finally, improved control and model settings for CO emission limiting combustion are discussed and measurements are presented before the paper concludes with a summarizing discussion.

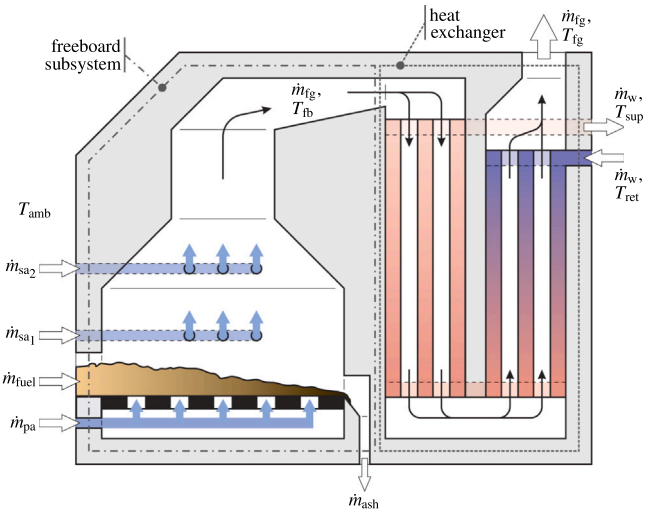

Fig. 1. Basic furnace structure with the most important mass flows and temperatures required for modeling. The furnace is split into the freeboard subsystem and the heat exchanger.

2. Furnace model

This section introduces the basic furnace design, the underlying process model and provides a short overview of emission formation for small-scale biomass grate furnaces. A basic description of the furnace and the process model is given in [4] and of the specific CO formation process in [5], but important information is recapitulated for consistent readability. Adaptions made to the model used for control design are also presented and discussed in this section.

2.1. Process description

The investigated plant is a small-scale grate furnace, as depicted schematically in Fig. 1 that is designed for the combustion of wood pellets or chips. Other fuel types are possible as well if they are provided in small pieces that can be managed by the conveyor system. Inputs to the furnace are the mass flow of wet fuel $\dot{m}_{fuel}$, the primary air mass flow $\dot{m}_{pa}$ and the secondary air mass flow $\dot{m}_{sa}$. The secondary air mass flow is split into $\dot{m}_{sa1}$, which enters the freeboard just above the grate, and $\dot{m}_{sa2}$ to support complete combustion in the freeboard. The water mass flow $\dot{m}_w$ of the heating circuit enters the heat exchanger with the return water temperature T_{ret} on the colder side and leaves the furnace as supply water temperature T_{sup} on the hotter side. The spread between these two temperatures is the main measure for the energy supplied by the furnace to the heating circuit. For the investigated system, the water mass flow $\dot{m}_w$ and the return temperature T_{ret} are kept constant on the test rig, but they can be part of the controlled system. The return water temperature can be included in the state space system of the predictive controller as a measured disturbance for compensation. The water mass flow on the other hand has to be estimated if required since typically no measurements are available for small-scale furnaces. Therefore, the supply water temperature demand $T_{sup,ref}$ is the determining value of the furnace.

The air mass flows of the plant are not controllable independently. All three mass flows depend on the fan speed of the single fan in the exhaust system, which pulls the air through the furnace. The secondary air mass flow 2 can be adjusted by an additional flap, which allows shutting down $\dot{m}_{sa2}$ almost completely. Geometric relations of the flow system however allow for an explicit constant ratio between $\dot{m}_{pa}$ and $\dot{m}_{sa1}$, which is typically adjusted during the installation of the furnace. This ratio contains empirical fuel-specific knowledge for the air mass flows and theoretically requires manual adjusting for different fuel types due to the existing feedforward control.

2.2. Modeling equations

The equations presented in this subsection are based on the energy and mass balances presented in [4] in order to obtain simple but descriptive relations for the model-based controller. Benefits of this model are the thoroughly investigated estimability of the gray-box parameters, the simplified thermal radiation terms and the small number of states. The following only contains the state equations necessary for control and minor adaptions to the original model.

2.2.1. Solid mass balance

The mass of fuel on the grate m_b is described by the balance equation

$$\frac{d}{dt}m_b = \dot{m}_{fuel,net} - \dot{m}_{thd}, \tag{1}$$

where $\dot{m}_{fuel,net}$ is the net mass flow of fuel available for combustion (in kg/s) and $\dot{m}_{thd}$ is the thermally decomposed fuel mass leaving the grate in a gaseous state over time (in kg/s). Due to the coupled air mass flows $\dot{m}_{pa}$ and $\dot{m}_{sa1}$, the primary air mass flow is expressed in terms of

$$\dot{m}_{pa} = r_{p2s1}\dot{m}_{psa}, \tag{2}$$

where $\dot{m}_{psa}$ is the combined mass flow of the primary and secondary air 1 (in kg/s) and r_{p2s1} is the geometric factor accounting for the fuel dependent air distribution of the furnace. The secondary air mass flow 1 is then given by

$$\dot{m}_{sa1} = (1 - r_{p2s1})\dot{m}_{psa}. \tag{3}$$

2.2.2. Oxygen concentration in flue gas

The oxygen concentration O_2 of the gaseous part after the combustion is considered to be finished based on [15] is obtained as

$$T_{O_2}\frac{d}{dt}O_2 = 21\frac{\lambda - 1}{\lambda} + k_{R_{thd}}\dot{R}_{thd} - O_2, \tag{4}$$

where T_{O_2} is the experimentally determined time constant of the oxygen sensor, λ is the air-to-fuel ratio and $k_{R_{thd}}$ is an experimentally determined gain for $\dot{R}_{thd}$, which is the rate of change for the thermal decomposition (in kg/s). This additional state is considered to account for the fast dynamics of the oxygen concentration and is given by

$$\frac{d}{dt}R_{thd} = \dot{m}_{thd} - \zeta\, R_{thd}, \tag{5}$$

where ζ is 1/s and accounts for the correct representation of the physical units.

2.2.3. Freeboard gas temperature

The freeboard gas temperature T_{fb} is obtained from the energy balance of the freeboard subsystem as

$$m_g c_{p,g}\frac{d}{dt}T_{fb} = \dot{Q}_{in} + \dot{Q}_{comb} - \dot{Q}_{gas} - \dot{Q}_{rad}, \tag{6}$$

where m_g is the gas mass in the freeboard (in kg), $c_{p,g}$ is the specific heat capacity of the hot gas (in J kg/K), $\dot{Q}_{in}$ is the enthalpy transported into the furnace by the fuel and combustion air (in W), $\dot{Q}_{comb}$ is the energy released due to combustion (in W), $\dot{Q}_{gas}$ is the enthalpy flow of the hot gas leaving the freeboard (in W) and $\dot{Q}_{rad}$ are the radiation losses (in W).

2.2.4. Supply water temperature

Adaptions to the model derived in [4] are made focusing on the description of the supply water temperature T_{sup} and the temperature of the exhaust gas T_{ex}, which were both considered as states for the controller. Because these variables are coupled and based on the intention to use a simplified heat exchanger model, the exhaust air temperature is not considered as a state variable, but described by an algebraic relation instead. The supply water temperature T_{sup} is obtained as

$$m_{w,he}\bar{c}_{p,w}\frac{d}{dt}T_{sup} = \dot{Q}_w - \dot{m}_w\bar{c}_{p,w}\left(T_{sup} - T_{ret}\right) + k_{sup}, \tag{7}$$

where $m_{w,he}$ is the mass of water in the heat exchanger (in kg), $\bar{c}_{p,w}$ is the specific averaged heat capacity of water (in J kg/K), $\dot{Q}_w$ is the heat flow of water (in W), $\dot{m}_w$ is the water mass flow of the heating circuit and k_{sup} is an experimentally determined constant temperature offset (in K). The water heat flow is obtained similar to [8] as

$$\dot{Q}_w = k_{Q,1}\left[\dot{m}_{fg}\left(T_{fb} - \bar{T}_w\right)\right]^{k_{Q,2}} + \dot{Q}_{rec}, \tag{8}$$

where $k_{Q,1}$ and $k_{Q,2}$ are experimentally determined constants to shape the thermal energy exchange, $\bar{T}_w$ is the averaged water temperature in the heating circuit (in K) and $\dot{Q}_{rec}$ is the radiation recuperation (in W). Although the combination of the parameters $k_{Q,1}$ and $k_{Q,2}$ can cause difficulties in their estimation, the relation is quite flexible to be adjusted to measurements. The exhaust gas temperature T_{ex} is approximated by an algebraic equation similar to [25] as

$$T_{ex} = T_{fb} - \frac{\dot{Q}_w}{\dot{m}_{fg}\bar{c}_{p,fg}}, \tag{9}$$

where $\bar{c}_{p,fg}$ is the constant averaged heat capacity of the flue gas. This relation presents a sufficient description for T_{ex}, since it is not utilized for furnace control but only to monitor if condensation of the flue gas occurs.

2.3. Emission formation

In order to achieve emission limiting control, the formation of the most relevant emissions for the given furnace has to be considered. CO, NO_x and other trace gases are measured on the test rig by a nondispersive infrared sensor and are available offline for modeling and evaluation. Additional CO or NO_x measurements could be made available for control by combined CO- or NO_x-λ sensors, but model-based emission reduction strategies are to be preferred.

2.3.1. Nitrogen oxides

The release of NO_x for the combustion of wood pellets and chips depends on the temperature, the nitrogen content of the fuel and the combustion technology [14]. Reduced nitrogen concentrations are already achieved for the given furnace by air staging with substoichiometric conditions on the grate (λ<1) and excess air ratios in the freeboard (λ>1). Although temperature measurements are only available in the freeboard, thermal and prompt NO_x formation is assumed to be restricted due to temperature levels that never exceed 1000 K [15]. The remaining NO_x is mainly fuel-based and related to the amount of energy released. The required load determines the air ratios and the temperatures, resulting in an almost linear, load-dependent relation for the NO_x concentration which is presented in Section 4 together with closed-loop measurements. The available NO_x data is also presented in Fig. 2 for wood pellets and chips over the operating range of the freeboard temperature. The mostly linear relation can be translated into output constraints on the freeboard temperature for the MPC in order to limit NO_x.

2.3.2. Carbon monoxide

The formation of CO is a regular part of the combustion process. Provided enough oxygen, high temperatures and reaction time are available, carbon monoxide is oxidized almost completely to CO_2 in the freeboard. This is already achieved for nominal load at the given furnace. Static CO-λ diagrams show the averaged CO concentration in the flue gas as a function of the air-to-fuel ratio λ, the fuel type and/or the combustion temperature for a specific furnace. Such CO-λ characteristics are available in literature, e.g. in [1] or in [15] and typically reveal the optimal stationary operating conditions for minimal CO concentrations. In [5] dynamic and static models depending on the oxygen concentration O_2 and the freeboard temperature T_{fb} as inputs are derived for wood pellets. These black-box models provide dynamic estimates for a wide range of operating conditions based on the given combustion technology. Including such models into the prediction of

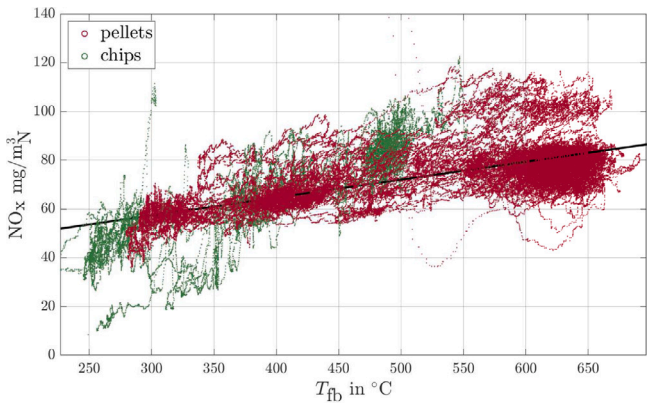

Fig. 2. Measured NO_x concentration in mg/m^3_N referenced to an oxygen concentration of 13 Vol.-% over the freeboard temperature T_{fb} in Celsius for wood pellets and chips. The black line represents a linear regression performed on the presented data to indicate the correlation with the operating temperature.

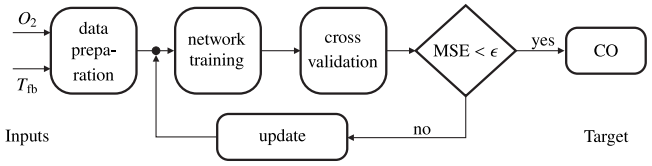

Fig. 3. Training procedure for the CO estimation model for wood pellets. The structure of the multilayer perceptron network is selected based on [5]. The network is trained, validated and updated in a loop until either the maximum number of iterations or a certain MSE is met. Because the model is static, different hold-out methods can conveniently be used for validation.

the MPC can provide a sophisticated approach for emission limiting control.

Simulation results of the model predictive controller with integrated dynamic CO models however have shown unsatisfactory performances due to high sensitivities of the output, especially with respect to disturbances in the oxygen concentration. This effect can be further amplified by inexpensive oxygen sensors that are commonly installed in small-scale furnaces which can show significant measurement errors. Furthermore, it is difficult to select setpoints or constraints for emissions, which are either unreasonable in general or cause conflicts with the more important setpoints for the furnace performance in terms of power. To prevent such conflicts and to keep the overall model as simple as possible, a static CO-O_2-T_{fb} map is utilized to derive a control strategy to limit the CO concentration through emission-related penalties instead.

This map is derived based on the results presented in [5], where several black-box modeling approaches are investigated and compared for the combustion of wood pellets. Inputs to the model are the measurements of O_2 and T_{fb} for which the parameterization procedure is displayed schematically in Fig. 3. A static multilayer perceptron network is trained and updated until a specific stopping criteria is met. Such approaches are utilized in different fields of engineering, e.g. for the estimation of mechanical properties [26], and are applicable to different furnaces as well since the measurements of O_2 and T_{fb} are usually always available for automated combustion processes. The obtained CO-O_2-T_{fb} estimation model or CO map for wood pellets is presented in Section 4.1 in Fig. 8 and validated together with the closed-loop measurements of the MPC in Section 4.3 in Figs. 9, 10, 14 and 15.

3. Controller design

This section provides the predictive control algorithm utilized at the investigated furnace and its application together with the already existing feedforward controller. The resulting architecture is depicted in Fig. 4 to provide a general understanding and is explained in detail throughout the following.

3.1. Application restrictions

The development of the MPC has to take the existing feedforward controller into account. Although this might limit the achievable potential of the newly developed controller, this fact also provides certain advantages. Because the given interfaces and settings are already defined, retrofitting the MPC to another furnace of the same design is straightforward. Additionally, because the existing feedforward control comprises the start-up, shut-down and safety features present at the furnace, they are kept in place without adaptions. Therefore, the model predictive controller can be considered as an "add-on" to the furnace. Nonetheless, the presented approach is applicable to the whole class of small-scale furnaces. Differences between applications with or without feedforward controller only arise in the MPC formulation relying on either absolute or relative values of the controllable inputs.

3.2. Extended furnace model

The presented model of the furnace together with empirically evolved software extensions constitute the extended furnace model as shown in Fig. 4, which is further introduced in the following. The extended furnace setup includes the input interface and the feedforward controller, which are briefly discussed in Sections 3.2.1 and 3.2.2, respectively.

3.2.1. Input interface

The most common control strategy for small-scale furnaces is based on independently designed control loops using simple linear PI controllers [15]. To achieve sufficient control performance with such an approach, decoupling of the process [27] and linear input–output behavior [28] are necessary prerequisites. In order to fulfill these requirements, the furnace manufacturer implemented the empirically designed input interface, which comprises hardware components (motors and valves) and an appropriately designed software to facilitate furnace operation. The so defined interface can be described as a four-dimensional look-up table given in concise form by the nonlinear mapping

$$\left[T_{\mathrm{sup,ref}}(k)\ \ \boldsymbol{u}^{\mathrm{T}}(k)\right] \mapsto \left[\dot{m}_{\mathrm{fuel}}(t)\ \ \dot{m}_{\mathrm{pa}}(t)\ \ \dot{m}_{\mathrm{sa}_1}(t)\ \ \dot{m}_{\mathrm{sa}_2}(t)\right] \tag{10}$$

with the vector $\boldsymbol{u}$ according to

$$\boldsymbol{u} = \left[u_{\mathrm{fuel}}\ \ u_{\mathrm{pa}}\ \ u_{\mathrm{sa}}\right]^{\mathrm{T}}. \tag{11}$$

While the subfigure in Fig. 4 shows how this mapping is integrated in the overall control concept, Fig. 5 shows explicit three-dimensional plots constituting the mapping of the input interface. Each of these plots visualizes a projection of the four-dimensional input vector to two inputs. The actual mass flows are thus obtained by interpolating within the complete four-dimensional look-up table. The supply temperature demand $T_{\mathrm{sup,ref}}$ influences this transformation in such a nonlinear way, that the process considering only the remaining input vector $\boldsymbol{u}$ is decoupled and exhibits linear input–output behavior. As long as the actual supply temperature is close to the reference value, these conditions are fulfilled in an appropriate but still approximate manner. Consequently, the vector $\boldsymbol{u}$ represents the controllable inputs of the extended furnace. Although the scalar inputs $\boldsymbol{u}$ basically lack a direct physical interpretation, they are labeled by indices referring to their main influence on the actual mass flows.

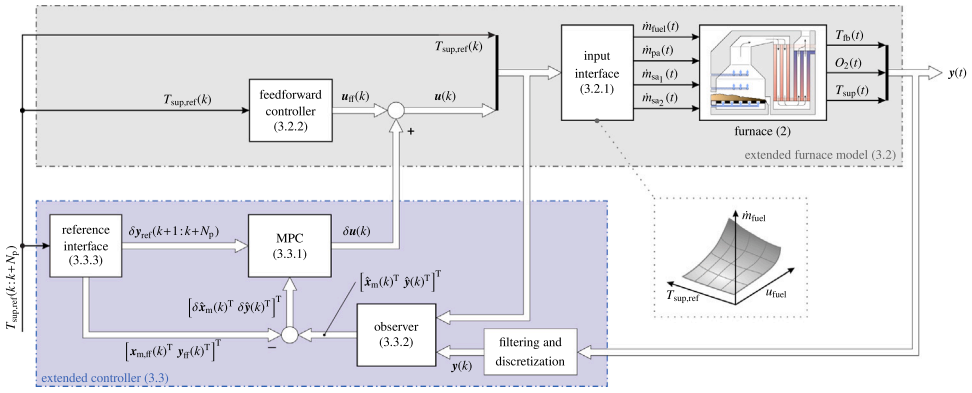

Fig. 4. Conceptual architecture of the overall control structure. The presented furnace, the input interface and the feedforward controller together constitute the extended furnace model. The extended controller comprises the MPC, the state observer, and the interface providing the necessary reference values. Applied filtering and discretization transforms measured time-continuous outputs $\boldsymbol{y}(t)$ into its time-discrete counterparts $\boldsymbol{y}(k)$. Numbers in brackets refer to the sections describing the corresponding block.

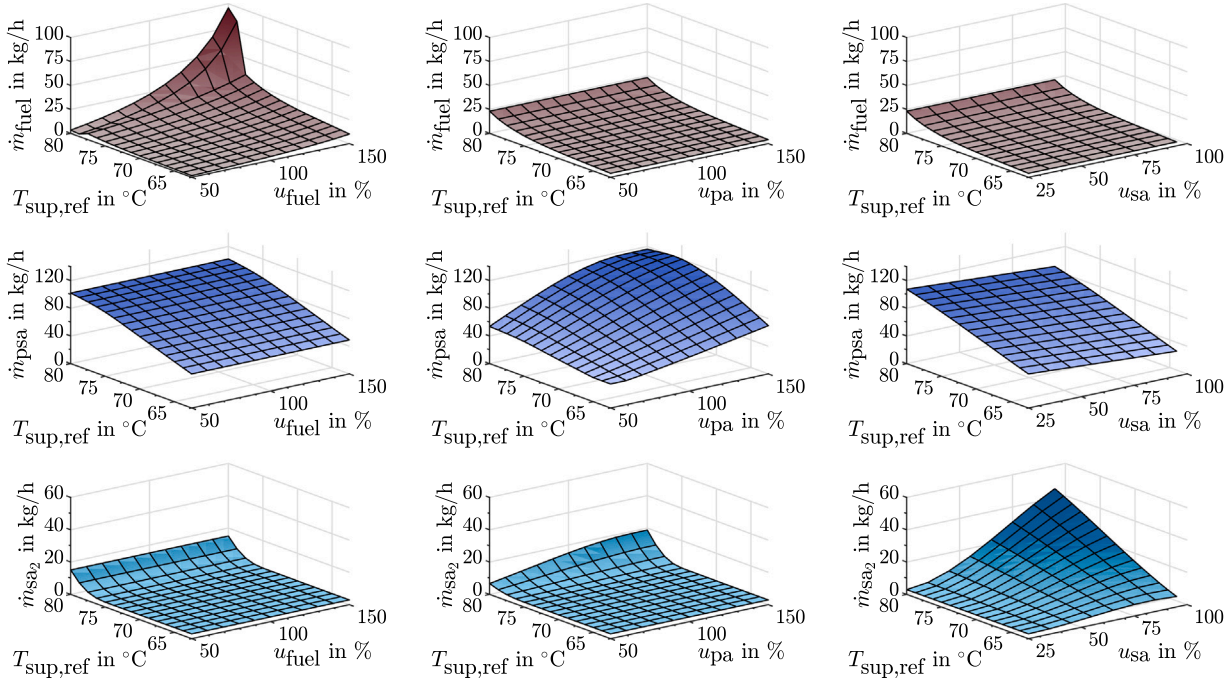

Fig. 5. Illustration of the relations within the input interface. While each column considers the influence of $T_{sup,ref}$ and one item of $\boldsymbol{u} = \left[u_{fuel}\ u_{pa}\ u_{sa}\right]^T$, mass flows are organized line-by-line. To allow depicted simplified representation, remaining values of $\boldsymbol{u}$ are chosen according to Eq. (12) in each diagram. Note that $\dot{m}_{psa}$ can be split up into $\dot{m}_{pa}$ and $\dot{m}_{sa_1}$ according to Eqs. (2) and (3), respectively.

3.2.2. Feedforward controller

The feedforward controller is designed empirically by the furnace manufacturer and is realized as a database of static fuel dependent tables. The applied static projection can be written in abbreviated form as

$$T_{sup,ref} \mapsto \boldsymbol{u}_{ff} = \left[u_{fuel,ff}\ \ u_{pa,ff}\ \ u_{sa,ff}\right]^T, \tag{12}$$

and is depicted in Fig. 6, which presents the settings applied for wood pellets. Based on the current fuel, the supply temperature reference $T_{sup,ref}$ defines feedforward actuator settings $\boldsymbol{u}_{ff}$, which are experimentally determined settings enabling high combustion quality for undisturbed combustion. Therefore, the MPC has to provide a feedback driven deviation term $\delta\boldsymbol{u}$ in addition to $\boldsymbol{u}_{ff}$. The combined feedforward and feedback control input $\boldsymbol{u}$ is thus obtained as

$$\boldsymbol{u} = \boldsymbol{u}_{ff} + \delta\boldsymbol{u}. \tag{13}$$

While performing trajectory planning in dynamic feedforward control would allow for designing the reference and disturbance behavior separately [29], the applied static input $\boldsymbol{u}_{ff}$ constrains the versatility of the system. The incapability of the static feedforward part to consider dynamic load changes forces the feedback controller to consider reference changes in a deviation-related fashion in addition to disturbance rejection. As the intended model predictive approach already includes the predictive property and therefore trajectory planning inherently, a dynamic extension of the existing static feedforward controller is not considered.

3.3. Extended controller

In addition to the emission limiting MPC, which is described in detail in Section 3.3.1, a state observer is necessary to estimate unmeasurable model states, which is briefly addressed in Section 3.3.2. Section 3.3.3 introduces the reference interface required to translate the supply temperature demand into the individual output references for the MPC. Because the control task requires these additional algorithms, the related blocks constitute the extended controller as shown in Fig. 4.

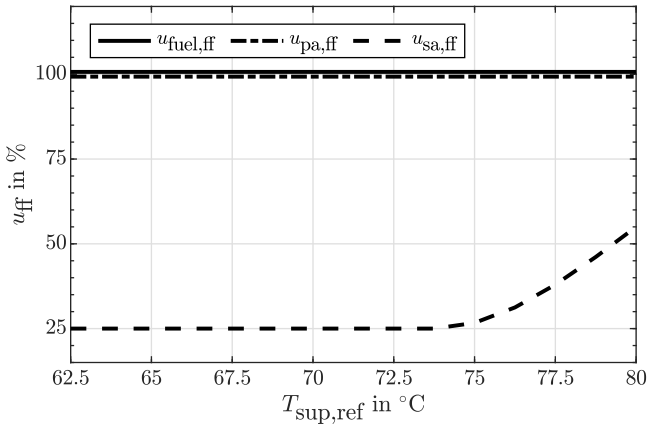

Fig. 6. Static feedforward relationship of Eq. (12) between $T_{\text{sup,ref}}$ and items in $\boldsymbol{u}_{\text{ff}}$ for the combustion of wood pellets.

3.3.1. MPC

Unconstrained formulation

Based on the state space representation of the augmented furnace (furnace and input interface) with the state vector $\boldsymbol{x}_{\text{m}} \in \mathbb{R}^{n_{\text{x}}}$, the output vector $\boldsymbol{y} \in \mathbb{R}^{n_{\text{y}}}$ according to Eq. (14), and the vector of controllable inputs $\boldsymbol{u} \in \mathbb{R}^{n_{\text{u}}}$, see Eq. (11), a linear MPC is established. The states and outputs are expressed as:

$$\begin{aligned} \boldsymbol{x}_{\text{m}} &= \left[m_{\text{b}}\ R_{\text{thd}}\ \text{O}_2\ T_{\text{fb}}\ T_{\text{sup}}\right]^T \\ \boldsymbol{y} &= \left[T_{\text{fb}}\ \text{O}_2\ T_{\text{sup}}\right]^T \end{aligned} \tag{14}$$

In order to obtain the necessary linearized furnace model, steady-state operating points resulting from feedforward control offer a wide range of potential linearization points. The ν-gap metric introduced by Vinnicombe [6] provides an appropriate method to compare different linear models regarding their deviation from each other in a closed-loop setting. Since $T_{\text{sup,ref}}$ is not included in the controllable input vector $\boldsymbol{u}$, the obtained linear models only differ slightly from each other in a ν-gap sense. This is due to the feedforward part, which covers most of the nonlinearities in the considered furnace setup due to the dependency on $T_{\text{sup,ref}}$. Thus, deviations from the selected linearization point are approximately equal to deviations from the steady-state operating point related to the feedforward control input $\boldsymbol{u}_{\text{ff}}$.

Based on these considerations and on the MPC formulation presented in [30], the discrete state space representation of the model used for control design can be written as

$$\begin{aligned} \delta\boldsymbol{x}_{\text{m}}(k+1) &= \boldsymbol{A}_{\text{m}}\,\delta\boldsymbol{x}_{\text{m}}(k) + \boldsymbol{B}_{\text{m}}\,\delta\boldsymbol{u}(k) + \boldsymbol{E}_{\text{m}}\,\delta d(k) \\ \delta\boldsymbol{y}(k) &= \boldsymbol{C}_{\text{m}}\,\delta\boldsymbol{x}_{\text{m}}(k) \end{aligned} \tag{15}$$

with the system matrix $\boldsymbol{A}_{\text{m}} \in \mathbb{R}^{n_{\text{x}} \times n_{\text{x}}}$, the input matrix $\boldsymbol{B}_{\text{m}} \in \mathbb{R}^{n_{\text{x}} \times n_{\text{u}}}$, the matrix $\boldsymbol{E}_{\text{m}} \in \mathbb{R}^{n_{\text{x}} \times n_{\text{d}}}$ of measured disturbances d and the output matrix $\boldsymbol{C}_{\text{m}} \in \mathbb{R}^{n_{\text{y}} \times n_{\text{x}}}$. The system presented in Eq. (15) is formulated in a deviation related fashion due to the existing feedforward controller. The matrix $\boldsymbol{E}_{\text{m}}$ accounting for the impact of the return water temperature $d = T_{\text{ret}}$ on the system can be omitted since T_{ret} is constant. In the following, the placeholder $(\star)$ therefore denotes the deviations δ from the steady-state operating points $(\star)_{\text{ff}}$ defined by feedforward control as

$$\delta(\star) = (\star) - (\star)_{\text{ff}}. \tag{16}$$

In order to eliminate steady-state offsets the plant model of Eq. (15) is augmented by adding n_{y} integrators. Applying the difference operation

$$\Delta(\star)(k+1) = \delta(\star)(k+1) - \delta(\star)(k) \tag{17}$$

yields the incremental formulation

$$\begin{aligned} \Delta\boldsymbol{x}_{\text{m}}(k+1) &= \boldsymbol{A}_{\text{m}}\,\Delta\boldsymbol{x}_{\text{m}}(k) + \boldsymbol{B}_{\text{m}}\,\Delta\boldsymbol{u}(k) \\ \delta\boldsymbol{y}(k+1) &= \delta\boldsymbol{y}(k) + \boldsymbol{C}_{\text{m}}\,\Delta\boldsymbol{x}_{\text{m}}(k+1) \end{aligned} \tag{18}$$

of the plant. With the augmented state vector

$$\boldsymbol{x}(k) = \begin{bmatrix} \Delta\boldsymbol{x}_{\text{m}}(k) \\ \delta\boldsymbol{y}(k) \end{bmatrix} \tag{19}$$

the state space representation of the augmented model is given by

$$\begin{aligned} \boldsymbol{x}(k+1) &= \boldsymbol{A}\boldsymbol{x}(k) + \boldsymbol{B}\Delta\boldsymbol{u}(k) \\ \delta\boldsymbol{y}(k) &= \boldsymbol{C}\boldsymbol{x}(k) \end{aligned} \tag{20}$$

with the matrices

$$\begin{aligned} \boldsymbol{A} = \begin{bmatrix} \boldsymbol{A}_{\text{m}} & \boldsymbol{0}_{n_{\text{x}} \times n_{\text{y}}} \\ \boldsymbol{C}_{\text{m}}\boldsymbol{A}_{\text{m}} & \boldsymbol{I}_{n_{\text{y}}} \end{bmatrix}, \quad \boldsymbol{B} = \begin{bmatrix} \boldsymbol{B}_{\text{m}} \\ \boldsymbol{C}_{\text{m}}\boldsymbol{B}_{\text{m}} \end{bmatrix}, \\ \boldsymbol{C} = \begin{bmatrix} \boldsymbol{0}_{n_{\text{y}} \times n_{\text{x}}}\ \boldsymbol{I}_{n_{\text{y}}} \end{bmatrix}, \end{aligned} \tag{21}$$

where $\boldsymbol{I}$ denotes an identity matrix and $\boldsymbol{0}$ a zero matrix of appropriate size. With N_{c} as the control horizon and N_{p} as the prediction horizon, the vectors of stacked incremental inputs $\Delta\boldsymbol{U}$ and stacked predicted outputs $\boldsymbol{Y}$ are defined as

$$\Delta\boldsymbol{U} = \left[\Delta\boldsymbol{u}(k)^{\text{T}}\ \ \Delta\boldsymbol{u}(k+1)^{\text{T}}\ \ \ldots\ \ \Delta\boldsymbol{u}(k+N_{\text{c}}-1)^{\text{T}}\right]^{\text{T}}, \tag{22}$$

$$\boldsymbol{Y} = \left[\delta\boldsymbol{y}(k+1|k)^{\text{T}}\ \ \delta\boldsymbol{y}(k+2|k)^{\text{T}}\ \ \ldots\ \ \delta\boldsymbol{y}(k+N_{\text{p}}|k)^{\text{T}}\right]^{\text{T}}, \tag{23}$$

respectively. Thus, the prediction can be written compactly as

$$\boldsymbol{Y} = \boldsymbol{F}\boldsymbol{x}(k) + \boldsymbol{\Phi}\,\Delta\boldsymbol{U}, \tag{24}$$

where the matrices are given by

$$\boldsymbol{F} = \left[(\boldsymbol{C}\boldsymbol{A})^{\text{T}}\ \left(\boldsymbol{C}\boldsymbol{A}^2\right)^{\text{T}}\ \ldots\ \left(\boldsymbol{C}\boldsymbol{A}^{N_{\text{p}}}\right)^{\text{T}}\right]^{\text{T}}, \tag{25}$$

$$\boldsymbol{\Phi} = \begin{bmatrix} \boldsymbol{C}\boldsymbol{B} & \boldsymbol{0}_{n_{\text{y}} \times n_{\text{u}}} & \cdots & \boldsymbol{0}_{n_{\text{y}} \times n_{\text{u}}} \\ \boldsymbol{C}\boldsymbol{A}\boldsymbol{B} & \boldsymbol{C}\boldsymbol{B} & \cdots & \boldsymbol{0}_{n_{\text{y}} \times n_{\text{u}}} \\ \boldsymbol{C}\boldsymbol{A}^2\boldsymbol{B} & \boldsymbol{C}\boldsymbol{A}\boldsymbol{B} & \cdots & \boldsymbol{0}_{n_{\text{y}} \times n_{\text{u}}} \\ \vdots & & & \\ \boldsymbol{C}\boldsymbol{A}^{N_{\text{p}}-1}\boldsymbol{B} & \boldsymbol{C}\boldsymbol{A}^{N_{\text{p}}-2}\boldsymbol{B} & \cdots & \boldsymbol{C}\boldsymbol{A}^{N_{\text{p}}-N_{\text{c}}}\boldsymbol{B} \end{bmatrix}. \tag{26}$$

With $\boldsymbol{Y}_{\text{ref}}$ as the vector of stacked references within the prediction horizon according to

$$\boldsymbol{Y}_{\text{ref}} = \left[\delta\boldsymbol{y}_{\text{ref}}(k+1)^{\text{T}}\ \ \delta\boldsymbol{y}_{\text{ref}}(k+2)^{\text{T}}\ \ \ldots\ \ \delta\boldsymbol{y}_{\text{ref}}(k+N_{\text{p}})^{\text{T}}\right]^{\text{T}} \tag{27}$$

the cost function J for optimization is determined by

$$J = \Delta\boldsymbol{U}^T\boldsymbol{R}_{\text{u}}\Delta\boldsymbol{U} + \left(\boldsymbol{Y}_{\text{ref}} - \boldsymbol{Y}\right)^T\boldsymbol{Q}_{\text{y}}\left(\boldsymbol{Y}_{\text{ref}} - \boldsymbol{Y}\right) + J_{\text{sc}}, \tag{28}$$

where the term J_{sc} accounts for additional costs due to soft constraints and is yet to be defined. The weighting matrices $\boldsymbol{R}_{\text{u}}$ and $\boldsymbol{Q}_{\text{y}}$ represent costs for increasing control inputs and to penalize control errors. Minimizing the cost function of Eq. (28) without considering constraints yields the optimal control sequence $\Delta\boldsymbol{U}^*$ according to

$$\Delta\boldsymbol{U}^* = \left(\boldsymbol{\Phi}^{\text{T}}\boldsymbol{Q}_{\text{y}}\boldsymbol{\Phi} + \boldsymbol{R}_{\text{u}}\right)^{-1}\boldsymbol{\Phi}^{\text{T}}\boldsymbol{Q}_{\text{y}}\left(\boldsymbol{Y}_{\text{ref}} - \boldsymbol{F}\boldsymbol{x}(k)\right). \tag{29}$$

The solution for the sequence of inputs $\Delta\boldsymbol{U}^*$ is obtained from solving the quadratic programming problem with the commercial software package MATLAB®.

Constraint formulation

The accessible solution space for the inputs is restricted by constraints on the amplitude of the inputs $\delta\boldsymbol{u}$, which must be chosen with respect to the absolute limits of $\boldsymbol{u}$. Based on the vector $\delta\boldsymbol{U}$, which combines the deviation-related inputs within the control horizon as

$$\delta\boldsymbol{U} = \begin{bmatrix} \delta\boldsymbol{u}(k) \\ \delta\boldsymbol{u}(k+1) \\ \vdots \\ \delta\boldsymbol{u}(k+N_{\text{c}}-1) \end{bmatrix} = \boldsymbol{T}_{\text{u},1}\,\delta\boldsymbol{u}(k-1) + \boldsymbol{T}_{\text{u},2}\,\Delta\boldsymbol{U} \tag{30}$$

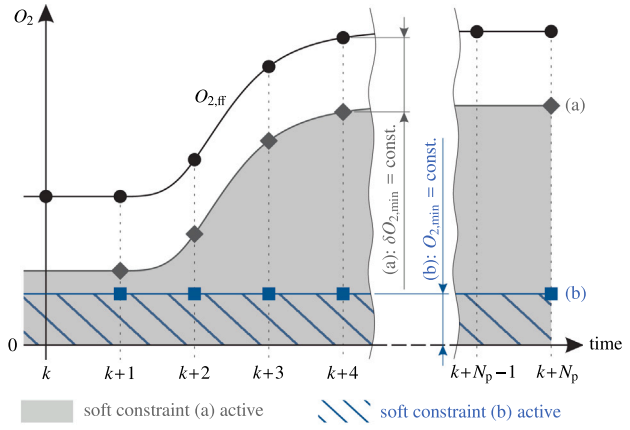

Fig. 7. Different options for the constraints imposed on O_2. While option (a) introduces a limit relative to the feedforward settings, option (b) restricts O_2 in an absolute fashion. The time-discrete values are connected smoothly to guide the eye.

with the matrices

$$\boldsymbol{T}_{\mathrm{u},1} = \begin{bmatrix} \boldsymbol{I}_{n_u} \\ \boldsymbol{I}_{n_u} \\ \vdots \\ \boldsymbol{I}_{n_u} \end{bmatrix} \quad \boldsymbol{T}_{\mathrm{u},2} = \begin{bmatrix} \boldsymbol{I}_{n_u} & \boldsymbol{0}_{n_\mathrm{u}\times n_\mathrm{u}} & \cdots & \boldsymbol{0}_{n_\mathrm{u}\times n_\mathrm{u}} \\ \boldsymbol{I}_{n_u} & \boldsymbol{I}_{n_u} & \cdots & \boldsymbol{0}_{n_\mathrm{u}\times n_\mathrm{u}} \\ \vdots & & & \\ \boldsymbol{I}_{n_u} & \boldsymbol{I}_{n_u} & \cdots & \boldsymbol{I}_{n_u} \end{bmatrix}, \tag{31}$$

hard input constraints are expressed by

$$\boldsymbol{T}_{\mathrm{u},1}\delta\boldsymbol{u}_{\min} \leq \delta\boldsymbol{U} \leq \boldsymbol{T}_{\mathrm{u},1}\delta\boldsymbol{u}_{\max}. \tag{32}$$

Since the CO emissions strongly increase if the oxygen concentration falls below certain values, which is visible in Fig. 8 in Section 4.1 of the results, introducing a bottom limit for O_2 is reasonable to ensure high combustion quality. Hard limitations of output variables however can restrict the feasibility of the optimization problem. To penalize low O_2 levels, soft constraints are assigned to the vector of predicted deviation-related oxygen concentrations $\boldsymbol{Y}_{\mathrm{O2}}$, which are obtained from the according entries of $\boldsymbol{Y}$. In order to ensure feasibility, a slack variable $s \in \mathbb{R}^{0+}$ is introduced, yielding the condition

$$\boldsymbol{Y}_{\mathrm{O}_2} \geq \boldsymbol{Y}_{\mathrm{O}_2,\min} - s\,\boldsymbol{1}_{N_p\times 1} \tag{33}$$

with $\boldsymbol{Y}_{\mathrm{O}_2,\min}$ as the vector of minimum permissible oxygen concentrations within the prediction horizon and $\boldsymbol{1}$ denoting a matrix of ones of appropriate size. Fig. 7 presents two possible approaches to specify these limits in the given setting. Option (a) represents a constant limit $\delta\mathrm{O}_{2,\min}$ in the form of an offset relative to the steady-state oxygen concentration $\mathrm{O}_{2,\mathrm{ff}}$ and option (b) constitutes a constant absolute bottom limit $\mathrm{O}_{2,\min}$, independent of the actual operating point. Their mathematical implementations are given by Eqs. (34)(a) and (34)(b) respectively.

$$\boldsymbol{Y}_{\mathrm{O}_2,\min} = \begin{cases} \boldsymbol{1}_{N_p\times 1}\,\delta\mathrm{O}_{2,\min} & \text{(a)} \\ \boldsymbol{1}_{N_p\times 1}\,\mathrm{O}_{2,\min} - \boldsymbol{O}_{2,\mathrm{ff}}^{\mathrm{pred}} & \text{(b)} \end{cases} \tag{34}$$

The vector $\boldsymbol{O}_{2,\mathrm{ff}}^{\mathrm{pred}}$ is defined as

$$\boldsymbol{O}_{2,\mathrm{ff}}^{\mathrm{pred}} = \left[\mathrm{O}_{2,\mathrm{ff}}(k+1)\ \mathrm{O}_{2,\mathrm{ff}}(k+2)\ \ldots\ \mathrm{O}_{2,\mathrm{ff}}(k+N_\mathrm{p})\right]^{\mathrm{T}}. \tag{35}$$

and comprises steady-state oxygen concentrations based on the feedforward controller. Constraint option (a) represents a reasonable approach, if the feedforward settings already result in low emissions in steady-state operation. Experimental results together with the CO model however suggest oxygen references, which are different from those provided by the feedforward part. The applied soft constraints are further discussed in the results section. Both options however introduce the additional costs J_{sc}, as stated in Eq. (28), according to

$$J_{\mathrm{sc}} = c_1 s + c_2 s^2 \tag{36}$$

with $c_1, c_2 \in \mathbb{R}^{0+}$ allowing to influence the soft constraint's impact. Considering s as an additional decision variable, the overall quadratic cost function is augmented to

$$J = \begin{bmatrix} \Delta\boldsymbol{U} \\ s \end{bmatrix}^{\mathrm{T}} \boldsymbol{H} \begin{bmatrix} \Delta\boldsymbol{U} \\ s \end{bmatrix} + \boldsymbol{f}^{\mathrm{T}} \begin{bmatrix} \Delta\boldsymbol{U} \\ s \end{bmatrix} \tag{37}$$

with the matrices

$$\boldsymbol{H} = \begin{bmatrix} \boldsymbol{R}_{\mathrm{u}} + \boldsymbol{\Phi}^{\mathrm{T}}\boldsymbol{Q}_{\mathrm{y}}\boldsymbol{\Phi} & 0 \\ \boldsymbol{0}_{1\times N_\mathrm{c} n_\mathrm{u}} & c_2 \end{bmatrix}, \tag{38}$$

$$\boldsymbol{f}^{\mathrm{T}} = \left[-2\left(\boldsymbol{Y}_{\mathrm{ref}} - \boldsymbol{F}\boldsymbol{x}(k)\right)\boldsymbol{Q}_{\mathrm{y}}\boldsymbol{\Phi},\quad c_1\right]. \tag{39}$$

Eq. (37) is therefore subject to the inequality constraints expressed by

$$\begin{bmatrix} \boldsymbol{T}_{\mathrm{u},2} & \boldsymbol{0}_{N_\mathrm{c} n_\mathrm{u}\times 1} \\ -\boldsymbol{T}_{\mathrm{u},2} & \boldsymbol{0}_{N_\mathrm{c} n_\mathrm{u}\times 1} \\ -\boldsymbol{T}_{\mathrm{O}_2}\boldsymbol{\Phi} & -\boldsymbol{1}_{N_p\times 1} \\ \boldsymbol{0}_{1\times N_\mathrm{c} n_\mathrm{u}} & -1 \end{bmatrix} \begin{bmatrix} \Delta\boldsymbol{U} \\ s \end{bmatrix} \leq \begin{bmatrix} \boldsymbol{T}_{\mathrm{u},1}\left(\delta\boldsymbol{u}_{max} - \delta\boldsymbol{u}(k-1)\right) \\ \boldsymbol{T}_{\mathrm{u},1}\left(-\delta\boldsymbol{u}_{min} + \delta\boldsymbol{u}(k-1)\right) \\ \boldsymbol{T}_{\mathrm{O}_2}\boldsymbol{F}\boldsymbol{x}(k) - \boldsymbol{Y}_{\mathrm{O}_2,\min} \\ 0 \end{bmatrix} \tag{40}$$

with the transformation matrix $\boldsymbol{T}_{\mathrm{O2}}$ pointing only to oxygen. Eq. (40) constitutes the final quadratic programming problem. Due to the receding horizon principle, only the first entry of the solution for $\Delta\boldsymbol{U}^*$ obtained from optimization is applied.

3.3.2. Observer

Based on the furnace model, an extended Kalman filter is applied to estimate model states and outputs. The extended Kalman filter is applied because it is considered to be the standard approach for nonlinear observation and since no differences in the performance compared to an unscented Kalman filter have been observed. The estimated state vector $\hat{\boldsymbol{x}}_{\mathrm{m}}(k)$ and output vector $\hat{\boldsymbol{y}}(k)$ are combined to an augmented state vector $\hat{\boldsymbol{x}}(k)$ and replace $\boldsymbol{x}(k)$ in Eq. (29) and in the consecutive equations.

3.3.3. Reference interface

The reference interface as part of the extended controller has to provide an appropriate reference vector $\delta\boldsymbol{y}_{\mathrm{ref}}$ for the MPC according to

$$\delta\boldsymbol{y}_{\mathrm{ref}} = \begin{bmatrix} \delta T_{\mathrm{fb,ref}} \\ \delta O_{2,\mathrm{ref}} \\ \delta T_{\mathrm{sup,ref}} \end{bmatrix} = \boldsymbol{y}_{\mathrm{ref}} - \boldsymbol{y}_{\mathrm{ff}} \tag{41}$$

for every time step within the prediction horizon. Thereby, the absolute reference $\boldsymbol{y}_{\mathrm{ref}}$ is corrected by the steady-state value $\boldsymbol{y}_{\mathrm{ff}}$. Because the control algorithm is based on a deviation related formulation, the steady-state values, $\boldsymbol{x}_{\mathrm{m,ff}}$ and $\boldsymbol{y}_{\mathrm{ff}}$, have to be considered permanently. For this purpose, the reference interface uses an overall model of the process, consisting of the feedforward controller (Eq. (12)), the input interface (Eq. (10)), and the furnace (Eqs. (1)–(8)). In order to obtain the steady-state state and output values solely induced by feedforward control, these equations are solved stationarily for the applied supply temperature reference by setting all time derivatives to zero. The resulting nonlinear mappings can be written in abbreviated form as:

$$T_{\mathrm{sup,ref}}(k) \mapsto \boldsymbol{x}_{\mathrm{m,ff}}(k) \tag{42}$$

$$T_{\mathrm{sup,ref}}(k : k+N_\mathrm{p}) \mapsto \boldsymbol{y}_{\mathrm{ff}}(k : k+N_\mathrm{p}) \tag{43}$$

Since the return water temperature T_{ret} and water mass flow $\dot{m}_{\mathrm{w}}$ are both constant in the given furnace setup, the absolute heat power demand P_{ref} is directly proportional to the supply water temperature $T_{\mathrm{sup,ref}}$ given by

$$P_{\mathrm{ref}} = \dot{m}_{\mathrm{w}} c_{\mathrm{p,w}}\left(T_{\mathrm{sup,ref}} - T_{\mathrm{ret}}\right). \tag{44}$$

This relation further justifies utilizing $T_{\mathrm{sup,ref}}$ as the main reference value for control. Due to the static feedforward controller, harsh changes of P_{ref} cause rapid changes of the actuators as well. In order to prevent excessive excitations, the reference interface incorporates a moving average filter with a window length of 90 time steps to smoothen the references within the prediction horizon. Therefore, the applied relative oxygen constraint according to Eq. (33) based on Eq. (34)(a) becomes active 15 min before the steps occur as well.

4. Results and discussion

In the following, the closed-loop results for the combustion of different solid biofuels are presented. The results for the combustion of wood pellets are discussed first, after a short introduction of the general MPC setup. Fuel flexibility and emission limiting control are presented in the consecutive subsections.

4.1. Control setup

The main control objectives are providing a specific heat demand expressed by the supply water temperature T_{sup} and enabling a high combustion quality. The freeboard temperature T_{fb} is considered more as a result of these demands rather than an independently controlled variable. This is due to potential conflicts with the more important O_2 references in terms of emissions and efficiency. The impact of T_{fb} therefore is restricted to achieving steady-state setpoints and respecting constraints, but less so for transient behavior. This is realized by small weights for T_{fb}. Unless stated otherwise, the weighting matrices are set according to

$$R_{\mathrm{u}} = \mathrm{diag}([r_{\mathrm{fuel}}\ r_{\mathrm{pa}}\ r_{\mathrm{sa}}]) = \mathrm{diag}([10\ \ 2.5\ \ 1]), \tag{45}$$

$$Q_{\mathrm{y}} = \mathrm{diag}([q_{\mathrm{T_{fb}}}\ q_{\mathrm{O_2}}\ q_{\mathrm{T_{sup}}}]) = \mathrm{diag}([0.01\ \ 0.75\ \ 10]). \tag{46}$$

The MPC utilizes a prediction horizon of N_{p}=180 and a control horizon of N_{c}=90 time steps. The furnace system is sampled with $T_{\mathrm{s}} = 10\,\mathrm{s}$, thus yielding a prediction horizon of 30 min and a control horizon of 15 min. Adaptions to the weighting matrices R_{u} and Q_{y} are conducted based on results obtained from experiments, aiming for emission limited combustion control. The MPC is operated in MATLAB® over an interface provided by LabVIEW®, which itself is connected to the furnace bus-system. This setup allows to bypass the necessity to generate machine-interpretable code and allows quick adaptions to model and controller even during operation.

The emission related costs for the optimization of the MPC are based on the stationary outputs of the acquired CO estimation model for wood pellets, which is presented in Fig. 8. The combinations of O_2 and T_{fb} which result in the minimal CO concentration over the operating range are highlighted in red. Including this setpoint dependent path into the optimization of the MPC decreases the emissions optimally. Alternatively, a simpler but suboptimal path can be defined where the O_2 concentration is constant. This coincides with the CO-λ diagrams from literature, since the influence of T_{fb} can be neglected in most cases for the given furnace. For each temperature level, the projections of the CO-O_2 plane are therefore slices of CO-λ diagrams for different operating conditions. Both paths however represent a potential basis for the formulation of penalties in the optimization of the MPC to achieve emission limiting control, as elaborated in Section 3.3.1. The CO map can be obtained similarly for other furnaces and other fuel types as well, because the process described in Fig. 3 is generic and physically motivated. The CO map presented in Fig. 8 is thus only valid for wood pellets and a specific furnace, as the CO-λ diagrams are. Additionally, long term degradation and measurement uncertainties of the oxygen sensor can lead to deviations from the obtained map.

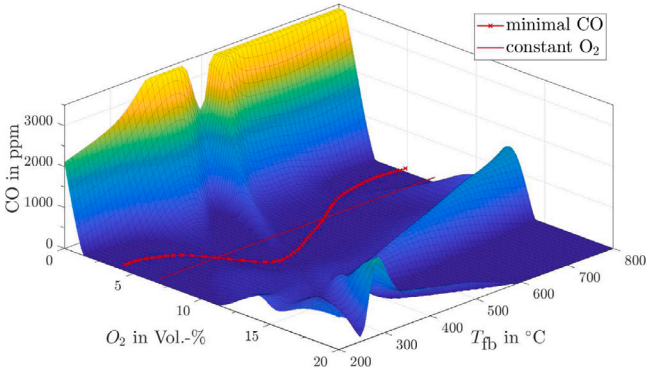

Fig. 8. Map of the CO concentration over the oxygen concentration O_2 and the freeboard temperature T_{fb} for wood pellets for the given furnace. The red line with stars highlights the path through the operating range resulting in the minimal CO concentration. The brown line represents a simpler suboptimal reference value of O_2 for low CO concentrations independent of T_{fb}.

4.2. Experimental setup

In order to compare the desired closed-loop results of the emission limiting MPC to the initial PI controller and for different fuels, the entire operating range of the furnace has to be investigated. This is conducted by a series of reference steps for $T_{\mathrm{sup,ref}}$ covering the supply water temperature levels of interest, starting at 100 kW nominal load and stepping through the operating range. The reference power is reduced to 50% and consecutively to 30% nominal load before it is increased to 100% load in the final step, which is the largest possible reference step realizable at the investigated furnace. All presented data obtained from different fuel types and controllers are generated for this profile and thus comparable, although the time between individual steps can differ slightly between experiments.

4.3. Initial closed-loop results for wood pellets

It is assumed, that the existing feedforward controller provides a reasonable steady-state combustion quality. The initial experiment settings therefore rely on the reference values $\boldsymbol{y}_{\mathrm{ref}}$ which are identical to the outputs $\boldsymbol{y}_{\mathrm{ff}}$ provided by the feedforward part. These references are the result of the heat demand expressed by $T_{\mathrm{sup,ref}}$ and the correlated values of P_{ref} according to Eq. (44). These references have not yet been optimized regarding emission formation. Closed-loop experiment data gathered from the application of the model predictive controller are presented in Fig. 9 for the combustion of wood pellets. The soft constraint for the oxygen concentration is set to $\Delta^{\mathrm{ff}}O_{2,\mathrm{min}} = 2\,\mathrm{Vol.\text{-}\%}$ according to Eq. (33) and option (a) of Eq. (34) with the initial cost coefficients being $c_1 = c_2 = 10$.

The results presented in Fig. 9 clearly indicate appropriate convergence towards reference values in steady state and satisfying transient behavior. In Section 4.5 a comparison between the simulated closed-loop results of the MPC and the currently employed PI control strategy shows that the implemented MPC in fact offers significant improvements as suggested in [4]. Among many aspects, the penalizing effect of the soft constraints contributes to this enhancement. Hard constraints have proven to be too harsh, whereas the influence of the soft constraints illustrates, that the oxygen concentration never falls significantly short of the applied limit.

Estimated CO emissions obtained from the soft-sensor according to Section 2.3 exhibit good agreement with measured values as shown in the second last diagram of Fig. 9. However, a considerable amount of CO emissions, especially occurring in the lower power range, indicate that the chosen references are inappropriate in terms of emissions. Peaks in the first hour are associated with low oxygen concentrations while increased CO emissions in the time span between 1 h and

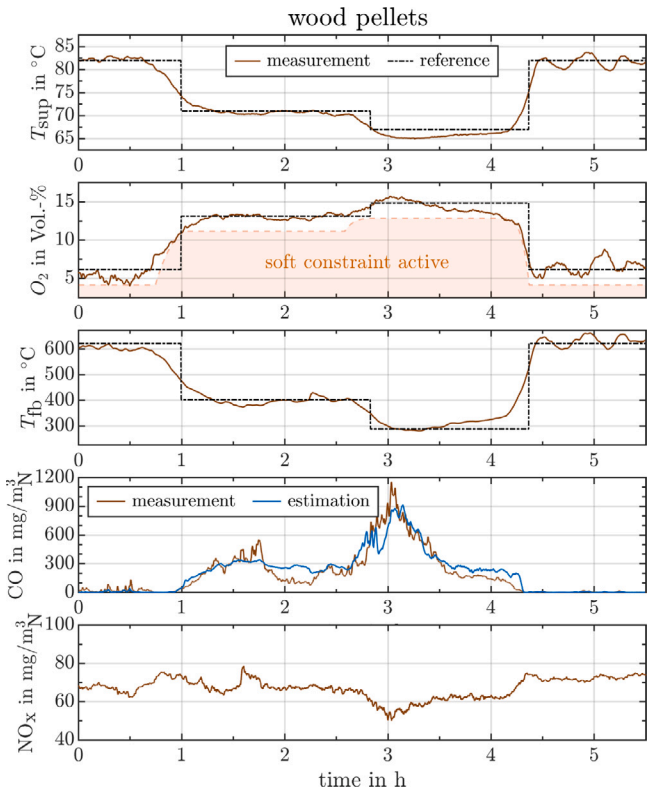

Fig. 9. Experimental closed-loop results for the combustion of wood pellets based on references supplied by the feedforward controller. The bottom plots show the measured and estimated emissions in the flue gas.

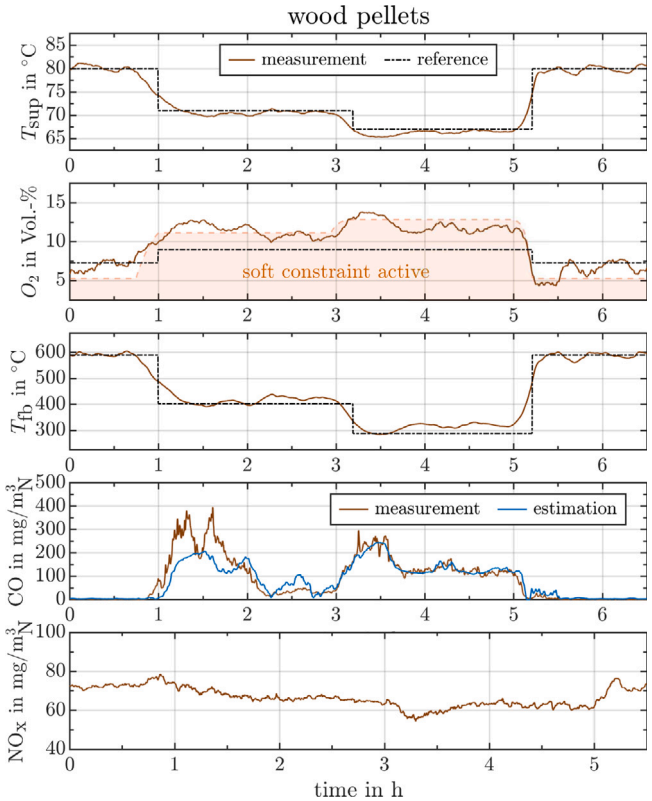

Fig. 10. Further experimental results for the combustion of wood pellets with slightly adapted O_2 references. The qualitative capabilities of the CO estimation model are validated in the second last plot.

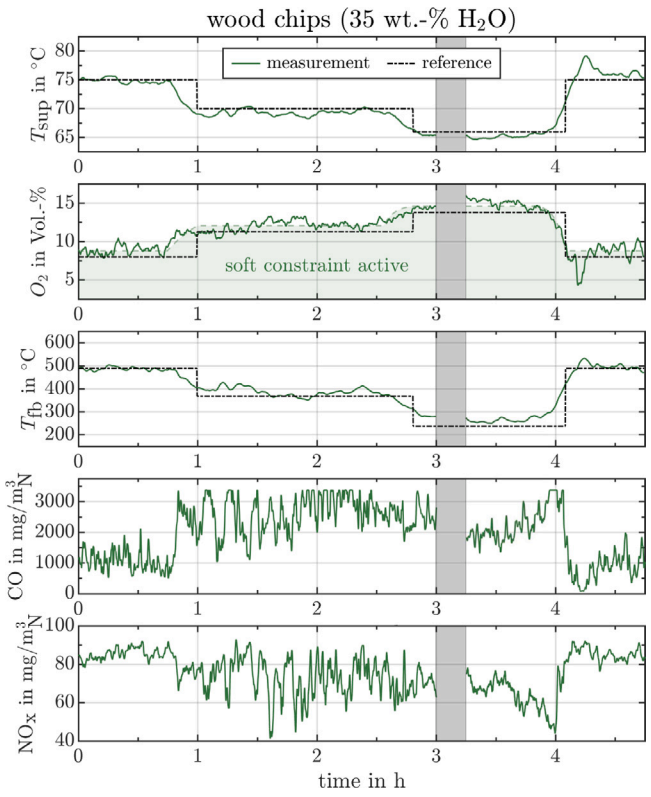

Fig. 11. Closed-loop results for the combustion of wood chips with a water content of 35 wt.-%. The references are supplied by the feedforward controller. The gray area indicates a short interruption due to grate cleaning.

4 h 15 min are the result of a low freeboard temperature T_{fb} and a relatively high O_2 concentration. These observations together with the CO map of Fig. 8 suggest to decrease the O_2 references during periods of lower power. Maintaining the same controller configuration but applying a slightly adapted O_2 reference yield the closed-loop results depicted in Fig. 10. While experimental results confirm the high estimation quality of the CO emission model, insufficient handling of the O_2 references highlights that constraints are partly situated by the MPC. Therefore, either the O_2 references or the soft constraints have to be adapted.

4.4. Fuel flexibility

Although the investigated furnace is mainly utilized for the combustion of wood pellets, minor changes of specific furnace settings allow other solid biofuels to be burned as well. This requires adjustments to the actuator settings of the furnace, which are expressed by the geometric ratio introduced in Eqs. (2)–(3) for the primary and secondary air mass flows. Updating the model parameters for a different fuel type is not necessary, if the expected water content of the fuel is approximately known. Therefore, based on the model parameters estimated for pellets, closed-loop results for the combustion of wood chips with water contents of 35 wt.-% and 20 wt.-% are obtained and displayed in Figs. 11 and 12, respectively.

The results for the combustion of wood chips with a water content of 35 wt.-% (Fig. 11) show a satisfying control performance by utilizing the unaltered controller settings. A short interruption due to furnace cleaning is highlighted by the gray areas in the figure, which required a restart in order to obtain the full measurement series. Based on the experiment data, small changes in the weighting factors of R_u and Q_y according to

$$r_{pa} = 0.5, \quad q_{O_2} = 3 \tag{47}$$

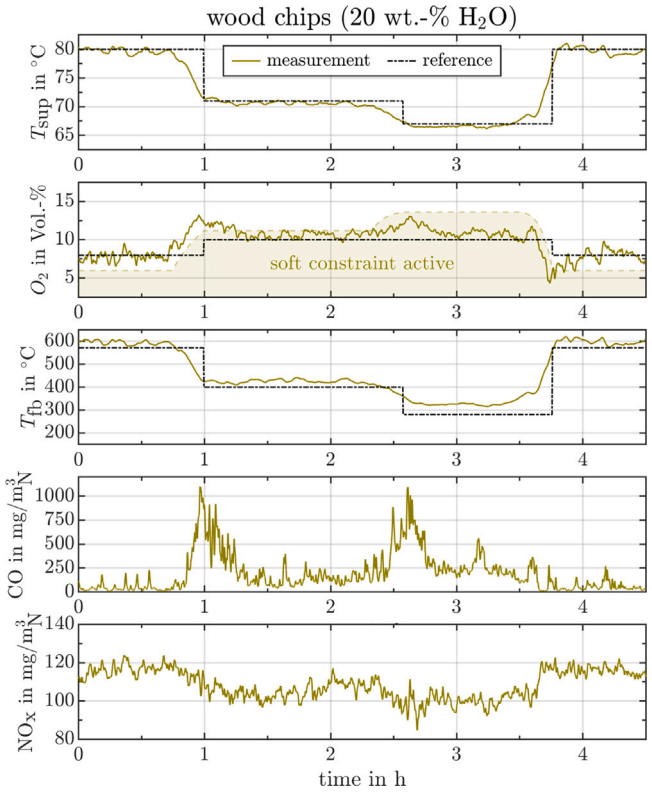

Fig. 12. Closed-loop experimental results for the combustion of wood chips with a water content of 20 wt.-% with slightly adapted O_2 references as applied in Fig. 10.

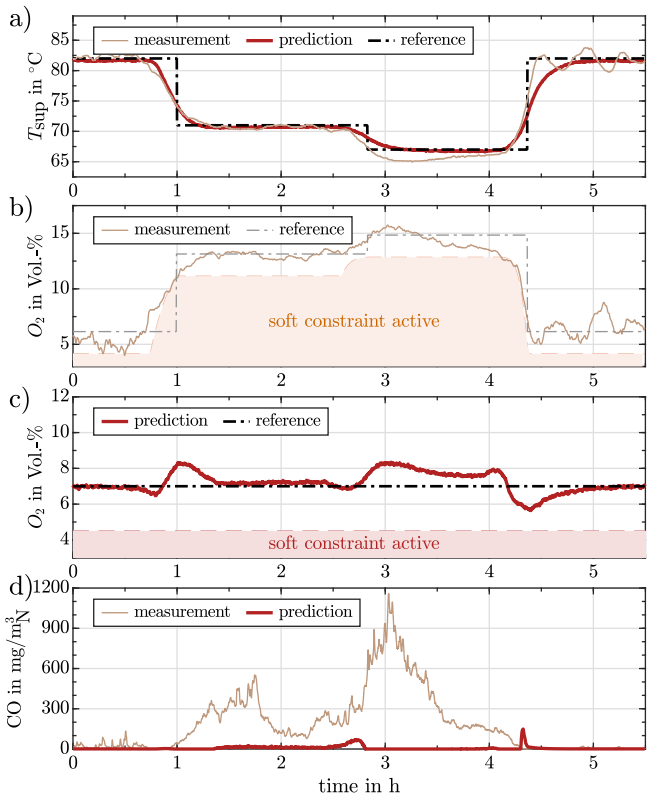

Fig. 13. Comparison between the initial closed-loop results for the combustion of wood pellets from Fig. 9 and the predicted results for the improved MPC based on simulation. The simulation is conducted with the adapted O_2 reference according to the CO reduction strategy, an absolute O_2 soft constraint and the adjusted weighting matrices of the MPC. The results for T_{sup} are compared in (a), whereas O_2 results are depicted separately in (b) and (c). In (d), the expected improvements of the CO concentration based on the predicted simulation is compared to the measurements obtained from the initial MPC settings.

are introduced, which yield the results depicted in Fig. 12 for wood chips with a water content of 20 wt.-%. The oxygen references in Fig. 11 have been unchanged compared to Fig. 9, whereas in Fig. 12 they have been altered towards lower levels. Due to the active O_2 soft constraint in Fig. 12, the control error increases in the time span between 2 h 30 min. and 3 h 45 min. Even though the soft constraints are permanently active for low temperatures, the MPC is able to reach the reference values. This shows, that the references for T_{sup} and O_2 can be selected independently to a certain degree and that the impact of the soft constraint is potentially too small.

Adjusting the soft constraints accordingly and fully incorporating sophisticated CO reduction strategies is expected to decrease the resulting emissions, especially for pellets, which is further discussed in the following section. The MPC configurations prove to be capable of controlling the combustion of different solid biofuels and providing a fast and effective approach for fuel switches through a minimal adaption of parameters, which could then be replaced by a fuzzy MPC for different fuels. The ability to control the supply temperature efficiently for different fuels is already a major improvement compared to the initial furnace control.

4.5. Emission limiting control

The application of the available CO models for wood pellets discussed in Section 2.3 describing the relations between O_2, T_{fb}, and CO offers a profound approach to find (sub)optimal O_2 references to minimize CO emissions. Fig. 8 reveals, that the dependency of the carbon monoxide concentration on the combustion temperature T_{fb} is rather small for some constant O_2 values. Deviations from these temperature levels are only penalized with slightly increased CO levels, whereas deviations of O_2 on the other hand can lead to very high CO concentrations. Therefore, a constant O_2 reference of 7 Vol.-% is determined to fulfill the objectives of simplicity and emission limitation, although the optimal path through the CO valleys of Fig. 8 is expected to yield better results. The CO model additionally reveals, that O_2 concentrations below 4.5 Vol.-% favor an excessively high CO formation, hence a bottom limit of $O_{2,min} = 4.5$ Vol.-% for the soft constraint according to Eqs. (33) and option (b) of Eq. (34) is applied. To enhance the new soft constraints and to refrain from hard implementing limits, the cost coefficients are set to $c_1 = c_2 = 10^5$.

Based on these considerations, a closed-loop simulation is utilized to investigate the expected improvements based on the available CO estimation model. The simulation results are depicted in Fig. 13 and compared to the already presented measurements shown in Fig. 9. The results for O_2 are presented separately in Figs. 13(b) and 13(c) for better visibility whereas T_{fb} is omitted. For the simulation, newly adapted MPC configurations are applied according to

$$R_u = \mathrm{diag}([2.5 \;\; 2.5 \;\; 1]), \tag{48}$$

$$Q_y = \mathrm{diag}([0.01 \;\; 20 \;\; 20]) \tag{49}$$

to better account for the importance of the oxygen concentration and to facilitate influence on the fuel mass flow, enhancing control performance. In Fig. 13(d) the simulation results of the predicted improvements of the CO concentration obtained with the updated controller tuning and the integrated CO strategy including new references are compared to the initially measured CO concentrations presented in Fig. 9. The resulting CO concentration is expected to be much lower with the updated settings than initially measured.

While shorter transition periods of T_{sup} for the first two reference steps assume a higher control performance with the adapted settings,

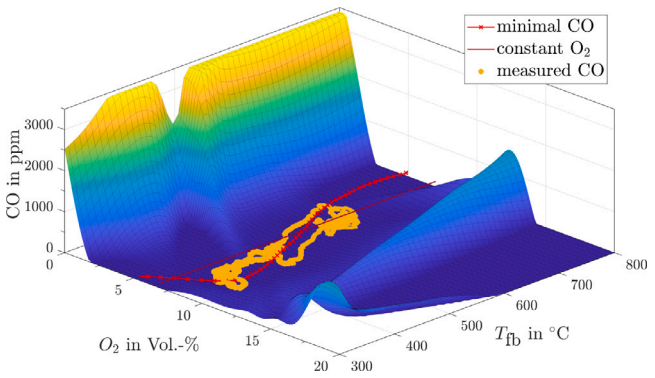

Fig. 14. CO map for wood pellets showing the experimental closed-loop results obtained with the final MPC settings presented in Fig. 15. The data highlights, that for the conducted dynamic sequence the individual measurements are located close to the minimal CO path and constant O_2 reference.

Table 1
Quantitative comparison of the control performance of the supply water temperature T_{sup} for the initial and the final MPC settings based on the RMSE together with the experiment duration.

Settings	RMSE (in °C)	Duration (in h)
PI initial	2.48	5.0
MPC final	1.51	5.0

the last and largest reference step shows a slightly increased rise time, see Fig. 13(a). As the underlying feedforward related actuator settings also exhibit these harsh changes, the MPC accepts a short activation of the soft constraints at 5 h 10 min in order to guarantee a smooth transition of the more important control goal of T_{sup}, which leads to a short CO peak in the simulation. The introduced intensified focus on the oxygen concentration however provides the intended emission reduction over the entire operating range, as presented in Fig. 13(d). Raising the lower oxygen limit $O_{2,min}$ towards the reference could decrease CO emissions during transition but simultaneously increase the rise time of T_{sup} as well. The expected trade-off between conflicting control goals prohibits further adaptions to the limits on O_2 since higher rise times can lead to unfavorable adjustments of the prediction horizon.

Finally, the experimental results for the intended emission limiting model predictive controller with fuel flexibility based on the discussed adaptions are presented in Fig. 14 showing the obtained CO measurements in the CO map and in Fig. 15 compared to the results obtained with the initial state-of-the-art PI controller. The resulting CO emissions are in fact vastly reduced based on the constant reference value of 7 Vol.-% for O_2 together with the soft constraints according to Eq. (34)(b) in comparison to the initial PI controller and to the MPC settings of Fig. 9. Especially in partial load operation, which is the case whenever T_{sup} is less than 80 °C, the CO emissions are reduced up to a factor of four. It is visible from the results, that the reference of the freeboard temperature T_{fb} needs to be reconsidered in terms of weighting or be redefined in general for the MPC. Although the higher temperature levels of T_{fb} might indicate an increased fuel consumption, the oxygen values and thus the mass flows of cold combustion air have been reduced as well.

To fully emphasize these improvements, Table 1 quantitatively compares the control performance of T_{sup} in terms of the root-mean-squared-error (RMSE) between the two controllers presented in Fig. 15. The RMSE allows an interpretation in the corresponding magnitudes, which are Celsius for the water temperature and mg/m^3_N ($O_{2,ref}$ = 13 Vol.-%) for the emissions.

Table 1 indicates, that the MPC considerably improved the control performance for the dynamic profile. Although the performance of the

Table 2
Quantitative comparison of the CO concentration in mg/m_{N^3} ($O_{2,ref}$=13 Vol.-%) between the initial state-of-the-art PI controller and the final MPC settings based on values averaged over the series of steps.

$T_{sup,ref}$ (load %)	Initial PI CO in mg/m_{N^3}	Final MPC CO in mg/m_{N^3}
80 °C+ (100%)	3.54	1.85
71 °C (50%)	39.98	24.34
67 °C (30%)	185.52	45.96
80 °C+ (100%)	7.14	1.68
Total avg.	59.04	18.46

PI controller is reasonable, the MPC achieves equal results in steady state but exceeds the PI during transition. The focus is however not to compare a PI controller with a predictive controller, but rather to highlight the incorporation of emission related control requirements. Therefore, similar to the comparison of T_{sup}, the measured CO emissions can be compared for these experiments as well. These results are presented in Table 2, showing the CO measurements averaged over the duration of the operating conditions according to the conducted series of steps.

Apparently, CO emissions have been reduced significantly in addition to the fact that the performance in terms of T_{sup} has not become worse but rather increased as well. The furnace settings for nominal load have already been well adjusted, which is highlighted by the fact that the PI feedback controller in Fig. 15 is even turned off in the gray areas. For partial load however, a favorable choice of references, constraints and weights for the MPC brings considerable improvements to the combustion quality, as presented. The obtained experimental results therefore show, that the introduced MPC setup considering emission limiting combustion indeed has the addressed potential to improve combustion control for existing furnaces.

5. Conclusion

This work introduced a model predictive controller for emission limiting small-scale biomass combustion for different fuel types based on staged combustion. Various results demonstrate the capability of the introduced methods in combination with the emission related considerations, which have been applied successfully to fuels with different properties. Due to the requirements stated by the already existing feedforward controller, the obtained MPC formulation can conveniently be retrofitted to furnaces of the same type without further adjustments or additional sensors.

The nonlinear furnace model introduced in Section 2 describes the combustion process adequately for the controller and the CO estimation model provided essential information about the emission formation process. Although in the final setting the CO model itself is not actively utilized, it has been essential to obtain the references for the oxygen concentration to highlight unfavorable operating conditions. Improvements to the CO model are expected to support the optimal choice of the O_2 references further. Limits on NO_x emissions can be achieved by constraining the upper limit of the freeboard temperature, at least for the considered combination of combustion technology and fuel.

The linear model predictive controller with the introduced mix of hard and soft constraints as presented in Section 3 proves to be sufficient for the investigated combustion process. A major part in smoothing the nonlinearities of the process is contributed by the existing feedforward controller, which prevents the necessity of a nonlinear controller design. However, the feedforward part also requires the derived controller to be defined in a deviation related formulation with respect to the provided steady-state inputs. In combination, these two controllers are able to provide reliable stationary operation for the entire furnace operating range.

While the original PI controller requires manual adjustment of the furnace hardware before operating with a different fuel, the derived

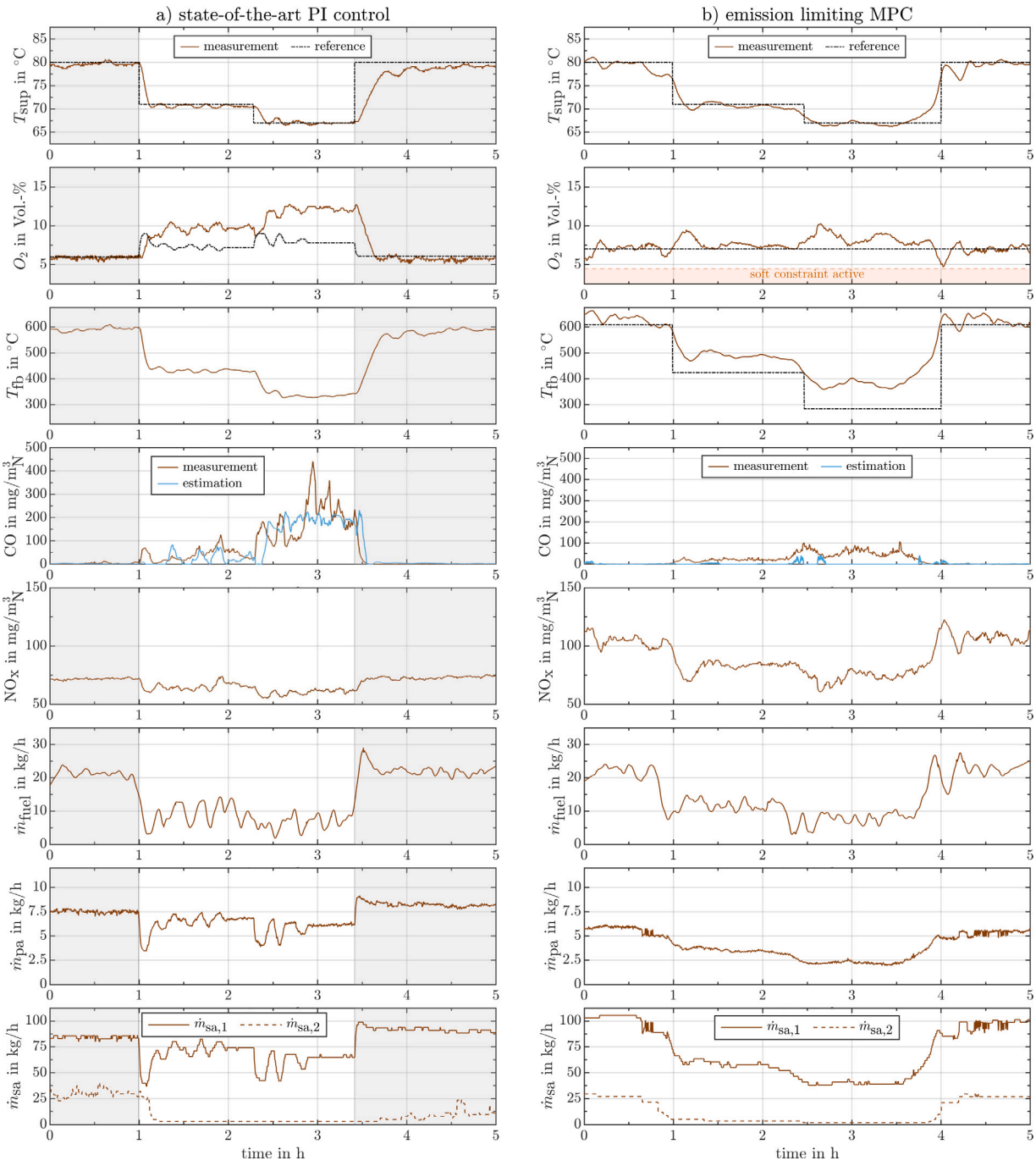

Fig. 15. Comparison of the experimental results obtained with the (a) state-of-the-art PI controller and the (b) emission limiting MPC. All relevant signals for a full comparison of the control algorithms are presented. The gray areas of the PI controller indicate that only feedforward control is active which has to be considered for the comparison of the controllers since the PI controller is not always fully active but the MPC has no such restrictions.

model predictive controller is able to cover the entire furnace operating range without hard adaptions. The acquired experimental results indicate, that further improvements can be achieved by fine adjustment of the weighting matrices of the MPC and a favorable choice of the output references. The development of the emission limiting MPC is not yet finished, but this work provides potential concepts. The optimal trade-off between heating performance, CO and NO_x emission reduction however has to be adapted to the specific requirements. An interesting considerable improvement would be to extend the furnace MPC with a soft-sensor for the water content or lower heating value of the fuel respectively, in order to further enhance robust control. The application of a fuzzy MPC could make use of additional CO maps for different fuel types or could eliminate manual interference with the process model at all.

A method has been formulated in this work for the operation of small-scale furnaces in an emission optimizing manner. The presented methodology is in general transferable to similar combustion systems, but special differences in technology and fuel require a precise examination of whether these measures are realizable or not. Caution should be taken when transferring the presented methods to other combustion processes: An important part of the strategy is that CO emissions can be reduced without an additional CO sensor. Based on a reliable CO map, operating conditions favoring low emissions can be identified. Prerequisites are robust oxygen sensors, which is however often not

the case for furnaces of smaller sizes because inexpensive sensors with significant measurement errors, especially on a long term basis, are common. Furthermore, for the presented two degrees of freedom controller and its application to other furnace systems, it is important that the feedforward controller describes the major nonlinearities of the process in order to allow an efficient linear feedback controller to be applied on the available hardware. It is therefore necessary that the feedforward control is valid for the entire range of operation or completely replaced by a MPC.

CRediT authorship contribution statement

Lukas Böhler: Conceptualization, Methodology, Software, Validation, Investigation, Data curation, Writing - original draft, Writing - review & editing, Visualization. **Markus Fallmann:** Software, Validation, Investigation, Data curation, Writing - original draft, Writing - review & editing, Visualization. **Gregor Görtler:** Software, Data curation, Investigation, Resources. **Jürgen Krail:** Conceptualization, Data curation, Investigation, Resources. **Florian Schittl:** Data curation, Investigation, Resources. **Martin Kozek:** Conceptualization, Methodology, Validation, Resources, Writing - review & editing, Supervision.

Declaration of competing interest

The authors declare that they have no known competing financial interests or personal relationships that could have appeared to influence the work reported in this paper.

Acknowledgments

The authors want to thank the partners at the FH-Burgen-land, Herz Energietechnik GmbH and Binder Energietechnik GmbH for their continuing support and the supply with experimental data of the furnace. This project (#853.606) is funded by the Climate and Energy Fund and conducted under the 2015 Energy Research Program.

References

[1] Fujii S, Tomiyama S, Nogami Y, Shirai M, Ase H, Yokoyama T. Fuzzy combustion control for reducing both co and nox from flue gas of refuse incineration furnace. JSME Int J C 1997;40(2):279–84.

[2] Korpela TM, Björkqvist TK, Lautala PA. Control strategy for small-scale wood chip combustion. IFAC Proc Vol (IFAC-PapersOnline) 2009;42(9):119–24. http://dx.doi.org/10.3182/20090705-4-SF-2005.00023.

[3] Peng H, Ozaki T, Toyoda Y, Shioya H, Nakano K, Haggan-Ozaki V, et al. RBF-ARX model-based nonlinear system modeling and predictive control with application to a NOx decomposition process. Control Eng Pract 2004;12(2):191–203. http://dx.doi.org/10.1016/S0967-0661(03)00050-9.

[4] Böhler L, Krail J, Görtler G, Kozek M. Fuzzy model predictive control for small-scale biomass combustion furnaces. Appl Energy 2020;276. http://dx.doi.org/10.1016/j.apenergy.2020.115339.

[5] Böhler L, Görtler G, Krail J, Kozek M. Carbon monoxide emission models for small-scale biomass combustion of wooden pellets. Appl Energy 2019;254(August):113668. http://dx.doi.org/10.1016/j.apenergy.2019.113668.

[6] Vinnicombe G. Uncertainty and feedback: H [infinity] loop-shaping and the [nu]-gap metric. World Scientific; 2001.

[7] Gölles M, Bauer R, Brunner T, Dourdoumas N, Obernberger I. Model based control of a biomass grate furnace. In: 9th European conference on industrial furnaces and boilers (2011), Vol. 1. 2011, p. 1–10.

[8] Gölles M, Reiter S, Brunner T, Dourdoumas N, Obernberger I. Model based control of a small-scale biomass boiler. Control Eng Pract 2014;22(1):94–102. http://dx.doi.org/10.1016/j.conengprac.2013.09.012.

[9] Schörghuber C, Gölles M, Reichhartinger M, Horn M. Control of biomass grate boilers using internal model control. Control Eng Pract 2020;96(May 2019):104274. http://dx.doi.org/10.1016/j.conengprac.2019.104274.

[10] Zemann C, Heinreichsberger O, Gölles M, Brunner T, Dourdoumas N, Obernberger I. Application of a model based control strategy at a fixed bed biomass district heating plant. In: 22nd European biomass conference and exhibition. 2014, p. 1678–705.

[11] Seeber R, Gölles M, Dourdoumas N, Horn M. Reference shaping for model-based control of biomass grate boilers. Control Eng Pract 2019;82(April 2018):173–84. http://dx.doi.org/10.1016/j.conengprac.2018.10.006.

[12] Paces N, Voigt A, Jakubek S, Schirrer A, Kozek M. Combined control of combustion load and combustion position in a moving grate biomass furnace. In: 2011 19th mediterranean conference on control and automation, MED 2011. 2011, p. 1447–52. http://dx.doi.org/10.1109/MED.2011.5983200.

[13] Kortela J, Jämsä-Jounela S-L. Model predictive control utilizing fuel and moisture soft-sensors for the biopower 5 combined heat and power (chp) plant. Appl Energy 2014;131:189–200.

[14] Nussbaumer T. Combustion and co-combustion of biomass: Fundamentals, technologies, and primary measures for emission reduction. Energy Fuels 2003;17(6):1510–21. http://dx.doi.org/10.1021/ef030031q.

[15] Kaltschmidt M, Hartmann H, Hofbauer H. Energie aus biomasse. Grundlagen, Techniken und Verfahren. Springer-Verlag Berlin-Heidelberg; 2016, 3. Auflage.

[16] Koppejan J, Van Loo S. The handbook of biomass combustion and co-firing. Routledge; 2012.

[17] Varol M, Atimtay AT, Olgun H, Atakül H. Emission characteristics of co-combustion of a low calorie and high sulfur-lignite coal and woodchips in a circulating fluidized bed combustor: Part 1. Effect of excess air ratio. Fuel 2014;117(PART A):792–800. http://dx.doi.org/10.1016/j.fuel.2013.09.051.

[18] Korpela T, Björkqvist T, Majanne Y, Lautala P. Online monitoring of flue gas emissions in power plants having multiple fuels. IFAC Proc Vol (IFAC-PapersOnline) 2014;19:1355–60. http://dx.doi.org/10.3182/20140824-6-za-1003.01913.

[19] Caposciutti G, Barontini F, Antonelli M, Tognotti L, Desideri U. Experimental investigation on the air excess and air displacement influence on early stage and complete combustion gaseous emissions of a small scale fixed bed biomass boiler. Appl Energy 2018;216:576–87. http://dx.doi.org/10.1016/j.apenergy.2018.02.125.

[20] Kalogirou SA. Artificial intelligence for the modeling and control of combustion processes: A review. In: Progress in energy and combustion science, Vol. 29. 2003, p. 515–66. http://dx.doi.org/10.1016/S0360-1285(03)00058-3.

[21] Chong AZ, Wilcox SJ, Ward J. Prediction of gaseous emissions from a chain grate stoker boiler using neural networks of ARX structure. IEE Proc: Sci Meas Technol 2001;148(3):95–102. http://dx.doi.org/10.1049/ip-smt:20010382.

[22] Thunman H, Leckner B. Co-current and counter-current fixed bed combustion of biofuel - A comparison. Fuel 2003;82(3):275–83. http://dx.doi.org/10.1016/S0016-2361(02)00289-2.

[23] Belkhir F, Meiers J, Felgner F, Frey G. A biomass combustion plant model for optimal control applications. In: 6th international renewable energy congress (IREC). 2015, http://dx.doi.org/10.1109/IREC.2015.7154075.

[24] Placek V, Sulc B. Support of biomass boiler control design by modeling. In: Proceedings of the 2015 16th international carpathian control conference, ICCC 2015. 2015, p. 393–8. http://dx.doi.org/10.1109/CarpathianCC.2015.7145111.

[25] Seeber R, Goelles M, Brunner T, Dourdoumas N, Obernberger I. Improvement of a model based control strategy for biomass furnaces. At-Automatisierungstechnik 2014;62(12):891–902.

[26] Hassanvand M, Moradi S, Fattahi M, Zargar G, Kamari M. Estimation of rock uniaxial compressive strength for an Iranian carbonate oil reservoir: Modeling vs. artificial neural network application. Pet Res 2018;3(4):336–45. http://dx.doi.org/10.1016/j.ptlrs.2018.08.004.

[27] Wang Q-G. Decoupling control, Vol. 285. Springer Science & Business Media; 2002.

[28] Charlet B, Lévine J, Marino R. On dynamic feedback linearization. Systems Control Lett 1989;13(2):143–51.

[29] Deutscher J. Zustandsregelung verteilt-parametrischer Systeme. Springer-Verlag; 2012.

[30] Wang L. Model predictive control system design and implementation using MATLAB®. Springer Science & Business Media; 2009.